INSTITUTE OF PHYSICS PUBLISHING JOURNAL OF PHYSICS: CONDENSED MATTER

J. Phys.: Condens. Matter **17** (2005) S3929–S3944 doi:10.1088/0953-8984/17/47/020

Actin-based motility: cooperative symmetry-breaking and phases of motion

A E Filippov[1], J Klafter[2] and M Urbakh[2]

[1] Donetsk Institute for Physics and Engineering of NASU, 83144, Donetsk, Ukraine
[2] School of Chemistry, Tel Aviv University, 69978 Tel Aviv, Israel

Received 8 July 2005
Published 4 November 2005
Online at stacks.iop.org/JPhysCM/17/S3929

Abstract

A microscopic model is proposed for the motility of a bead driven by the polymerization of actin filaments. The model exhibits a rich spectrum of behaviours similar to those observed in biomimetic experiments, which include spontaneous symmetry-breaking, various regimes of the bead's motion and correlations between the structure of the actin tail which propels the bead and the bead dynamics. The dependences of the dynamical properties (such as symmetry-breaking time, regimes of motion, mean velocity, and tail asymmetry) on the physical parameters (the bead radius and viscosity) agree well with the experimental observations. We find that most experimental observations can be reproduced taking into account only one type of filaments interacting with the bead: the detached filaments that push the bead. Our calculations suggest that the analysis of mean characteristics only (velocities, symmetry-breaking times, etc) does not always provide meaningful information about the mechanism of motility. The aim should be to obtain the corresponding distributions, which might be extremely broad and therefore not well represented by their mean only. Our findings suggest a simple coarse-grained description, which captures the main features obtained within the microscopic model.

1. Introduction

Biological movements display highly complex phenomena involving biochemical and biophysical processes [1]. Many of these movements are known to be driven by the polymerization of actin filaments, but their complete description is still missing. Significant progress in clarifying the molecular basis of actin-driven cell motility has been made by using biomimetic in vitro systems such as polystyrene beads (microspheres) coated with proteins that initiate actin polymerization [2–6].

The movement trajectories of polystyrene beads have been shown to be similar to those of bacterial pathogens such as *Listeria monocytogenes*, which have been used as model systems

for studies of actin-based motility [7, 8]. Beads are therefore helpful in getting some insight into the physical nature of actin-based motility. The major advantage of biomimetic systems is that they allow for quantitative measurements in which both biochemical and physical parameters can be controlled. Biomimetic systems have been used in order to investigate the actin tail formation, characterize the mechanism of symmetry breaking in cellular motion and explore the dynamical regimes of actin-based propulsion. The latter is further investigated by varying the surface concentration of the proteins which initiate actin polymerization, the size of the bead and the viscosity of the surrounding media [6].

Theoretical models are crucial for extracting biophysical information from experiments and then for understanding the mechanisms of force generation and motility that originate from actin polymerization. Experiments with biomimetic systems can in turn provide the possibility to test, and introduce improvements, into the various models. Recently, several theoretical models have been proposed which address the motility phenomena for cells and biomimetic systems on different scales. One class of models describes the phenomena on a microscopic level by considering the polymerization of a single filament, or a group of filaments, and their interaction with objects which represent *Listeria* or beads [9–12]. Another group of models explores a continuum approach considering the actin filament tails as an elastic gel [13–16]. In this case the coupling between polymerization and motion occurs due to the stress which is developed between the actin gel and the moving object. In spite of the recently growing theoretical efforts, both numerical and analytical, some questions are yet to be resolved in order to obtain a consistent picture of actin driven motility [6].

In this paper we propose a microscopic model that exhibits spontaneous symmetry-breaking and different regimes of bead motion. Using this model we study the effects of the experimentally controllable parameters, such as the radius of the bead and the viscosity of the surrounding medium, on the bead motility. Our findings lead to a coarse-grained continuous description, which captures the main features of the microscopic model and offers a complimentary description of the motility phenomena.

2. Microscopic approach

2.1. Model

The model we introduce assumes in accordance with experimental observations the presence of two populations of filaments: (1) *attached* filaments that pull the bead, and (2) *detached* filaments that polymerize and generate a pushing force. The filaments grow in the vicinity of a spherical bead which is propelled by the formation of a filament tail, see figure 1. The dynamics of the both filaments and the bead are treated via the Langevin description.

At each time step of the calculation the filaments are nucleated uniformly (on average) in a ring of radius $R_0 + \Delta R$ around the bead with probability $p_g \Delta t$, where R_0 is the radius of the bead. We denote a point of nucleation by $\mathbf{r}_i^s$, where the index i is a filament number. We assumed that one of the ends of the filament, $\mathbf{r}_i^s$, is attached to the cross-linked actin network and as a result it does not move, while the other end of the filament (barbed end) pushes or pulls the bead. Filaments which touch the bead are attached to it with probability $p_a \Delta t$, while the other filaments are treated as detached. The elongation of filaments can be described by the following Langevin equation:

$$\delta \mathbf{r}_i = \left[q_i \dot{\mathbf{R}} + \frac{1}{\gamma}(1 - q_i)\left(\mathbf{f}(\mathbf{r}_i - \mathbf{R}) + \xi_i(t)\right)\theta\left(|\mathbf{r}_i - \mathbf{R}| - R_0\right) \right] \Delta t. \tag{1}$$

The vectors $\boldsymbol{R}$ and $\boldsymbol{r}_i$ define the positions of the bead and of the end of the ith filament on its side close to the bead (barbed end), respectively. The parameter q_i characterizes the state

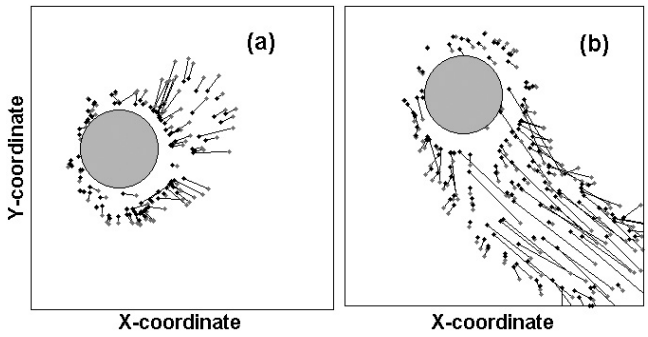

Figure 1. Distribution of filaments around a bead: (a) at the moment of the symmetry-breaking event and (b) during a directed motion of the bead. Black and grey points show the ends of the filaments close to the bead and to the nucleation points, respectively.

of an individual filament: $q_i = 1$ for the attached filaments and $q_i = 0$ for the detached ones. We assume that an attached filament is stretched with a velocity which is equal to the velocity of the bead, $\dot{\mathbf{R}}$, while a detached filament polymerizes in the direction towards the centre of the bead. The Heaviside step function, $\theta(z)$, takes into account that filaments cannot penetrate into the bead. The function $\mathbf{f}(\mathbf{r}_i - \mathbf{R}) = \frac{\mathbf{r}_i - \mathbf{R}}{|\mathbf{r}_i - \mathbf{R}|} f(|\mathbf{r}_i - \mathbf{R}|)\theta(|\mathbf{r}_i - \mathbf{R}| - R_0)$ determines the rate of polymerization, and as an example an exponential decay of f with a distance from the bead,

$$f(|\mathbf{r}_i - \mathbf{R}|) = A\,|\mathbf{r}_i - \mathbf{R}| \exp\left(-|\mathbf{r}_i - \mathbf{R}|^2/\lambda^2\right) \tag{2}$$

is assumed. Here A is the amplitude of the rate and λ is the characteristic width of the region around the bead where the polymerization occurs. The ratio $f(\mathbf{r}_i - \mathbf{R})/\gamma$, where γ is a dissipation constant, gives the velocity of polymerization. The effect of thermal fluctuations on the polymerization process is given by a random force $\xi_i(t)$, which is δ correlated in time $\langle \xi_i(t)\xi_j(0)\rangle = 2k_{\mathrm{B}}T\gamma\delta(t)\delta_{ij}$.

Each of the attached filaments is detached with probability $p_{\mathrm{d}}^0 \exp(Kl_i a/k_{\mathrm{B}}T)$, where p_{d}^0 is the spontaneous probability of detachment in a stress free state, K is the elasticity constant of a filament, l_i is the filament elongation after attachment, $l_i = |\mathbf{r}_i^a - \mathbf{r}_i|$, $\mathbf{r}_i^a$ is the point of attachment, and a is a characteristic width of the adhesion potential [17]. Each of the existing filaments is removed with probability $p_r\Delta t$. Notice that filament elongation is renewed every time after nucleation. Moreover, the instantaneous lengths and pushing and pulling forces are different for different filaments, and the number of working filaments also changes in time. Thus, the behaviour is not given by a mean field description which corresponds to a homogeneous picture.

The *detached* filaments push the bead with the force $F_1^{(i)}(\mathbf{r}_i - \mathbf{R}) = \frac{\mathbf{r}_i - \mathbf{R}}{|\mathbf{r}_i - \mathbf{R}|} F_1(|\mathbf{r}_i - \mathbf{R}|)$. Here we also assume an exponential decay with the distance from the bead,

$$F_1(|\mathbf{r}_i - \mathbf{R}|) = A_1\,|\mathbf{r}_i - \mathbf{R}| \exp\left(-|\mathbf{r}_i - \mathbf{R}|^2/\lambda^2\right) \tag{3}$$

with amplitude A_1 and the characteristic length λ. The *attached* filaments pull the bead back with the elastic force $F_2^{(i)} = -\frac{\mathbf{r}_i - \mathbf{r}_s}{|\mathbf{r}_i - \mathbf{r}_s|} K|\mathbf{r}_i^a - \mathbf{r}_i|$, where K is the stiffness of the filament and the vector $\frac{\mathbf{r}_i - \mathbf{r}_s}{|\mathbf{r}_i - \mathbf{r}_s|}$ defines the direction of the force along the filament.

On a macroscopic scale, focusing on the bead, the motion is governed by the following overdamped Langevin equation:

$$\tilde{\eta}\dot{\mathbf{R}} + F + \xi(t) = 0 \tag{4}$$

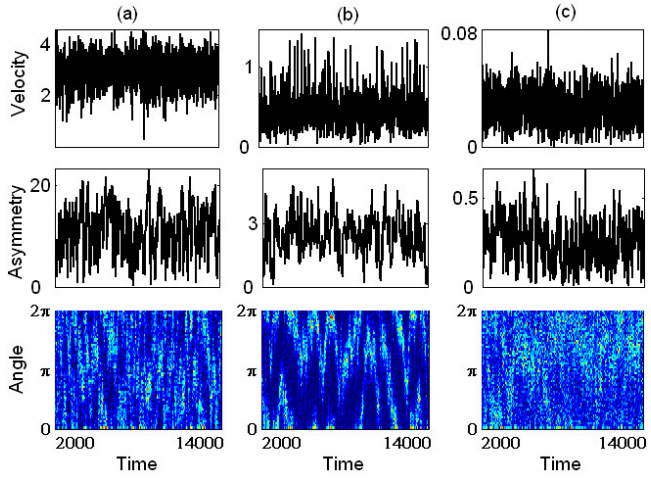

Figure 2. The time dependences of the bead velocity (absolute value of the velocity), the cloud asymmetry and angular distribution of actin filaments for three regimes of the bead motion: (a) steady motion of small beads, (b) hopping motion of the intermediate size beads, and (c) localized fluctuations of large beads. Light regions in the angular distributions correspond to maxima of the probability distribution function. Distances, velocity and time are presented in units of λ, $f(R_0)/\gamma$ and $\lambda\gamma/f(R_0)$, respectively. Parameter values: $A_1/A = 0.5$, $K/A = 0.05$, $6\pi\eta\lambda/\gamma = 1$, $K\lambda a/(k_B T) = 0.25$, $p_g = 3$, $p_a = 0.5$, $p_d^0 = 0.5$; (a) $-R_0/\lambda = 1$, (b) $-R_0/\lambda = 2$, (c) $-R_0/\lambda = 3$.

where

$$F = \sum_{i=1} \left[q_i F_2^{(i)} + (1 - q_i) F_1^{(i)} \right] \tag{5}$$

is the force due to the interaction between the filaments and the bead, the dissipation constant $\tilde{\eta}$ is related to a viscosity of surrounding medium through the Stokes equation, $\tilde{\eta} = 6\pi R_0 \eta$, and $\xi(t)$ is a δ-correlated random force acting on the bead, $\langle \xi(t)\xi(0) \rangle = 2k_B T \eta \delta(t)$. Equation (5) provides the total force experienced by the bead due to the dynamics of the filaments.

3. Results of simulations

Our simulations show that the above model exhibits three different types of bead motion, depending on the bead radius: (a) small beads move *steadily* with an almost constant velocity, (b) larger beads move in a *hopping* manner, and (c) a further increase of the bead radius leads to *localized* fluctuations of the bead within the actin cloud. In the transition region between steady and hopping motions the movement of the bead becomes erratic (jerky). The transitions from the steady motion of the bead to the hopping one and then to the trapped state with the increase of the bead radius have been recently observed experimentally [4]. These regimes of motion can be distinguished in figure 2 where the calculated time dependences of the bead velocity (absolute value of the velocity), of the cloud asymmetry and of the angular distribution of actin filaments are presented. The asymmetry is defined as the distance between the centre mass of the cloud and the centre of the bead, and an angular distribution of actin filaments is obtained by calculating the fraction of filaments around the bead which have a given direction (angle) with respect to a chosen frame, as shown in figure 3. The latter figure also presents an instantaneous angular density distribution of filaments in the hopping regime. In all figures

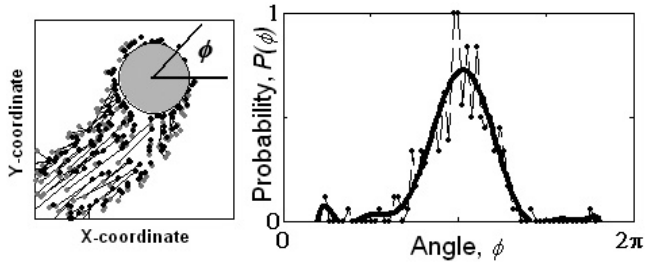

Figure 3. (a) Snapshot of a distribution of actin filaments from the time sequence shown in figure 2(b). (b) Filament density distribution as a function of angle for the frame shown in figure 3(a). Parameter values as in figure 2(b).

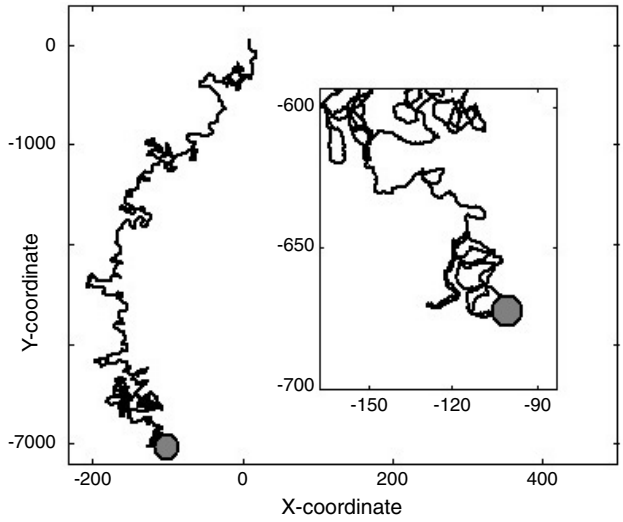

Figure 4. A typical bead trajectory in the hopping regime. The inset shows a part of the trajectory on an enlarged scale. Parameter values are as in figure 2(b).

corresponding to the microscopic model distances, time and velocity are presented in units of λ, $\lambda\gamma/f(R_0)$, and $f(R_0)/\gamma$, respectively.

Regimes of motion. Figure 2(a) demonstrates that small beads, $R_0/\lambda < 1.8$, never stop and that variations in the cloud asymmetry and of the angular distribution correspond to changes in the direction of the bead motion. In this case we find no correlation between all three characteristics (the bead velocity, the asymmetry and the angular distribution of the cloud).

In the hopping regime (figure 2(b)), which we find for the intermediate range of bead radii, $1.8 < R_0/\lambda < 2.5$, the bead performs jumps separated by time intervals during which it is trapped within a highly symmetric actin cloud. A typical bead trajectory in the hopping regime is shown in figure 4. In contrast to the steady motion case, here there are strong correlations among the bead velocity, cloud asymmetry and its angular distribution. Following an escape from a symmetric cloud (point A in figure 5) the bead starts to move with a high velocity (point B). Figure 5 clearly shows that an increase in velocity correlates with an increase in asymmetry of the actin cloud (point C). The continuum description presented below, in the next section, shows qualitatively that the directional motion of the bead generates an asymmetry

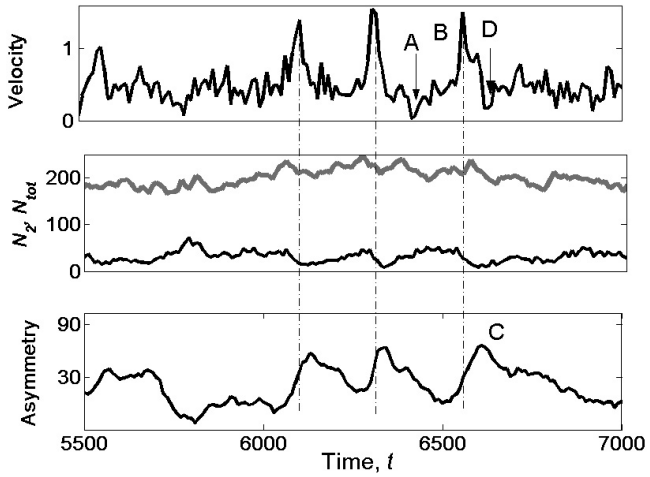

Figure 5. Time dependences of the bead velocity, the total number ($N_{\rm tot}$, grey line) of filaments and the number of attached (N_2, black line) filaments, and the cloud asymmetry in the hopping regime of the bead motion. The figure presents a segment of the time series shown in figure 2(b). Parameter values are as in figure 2(b).

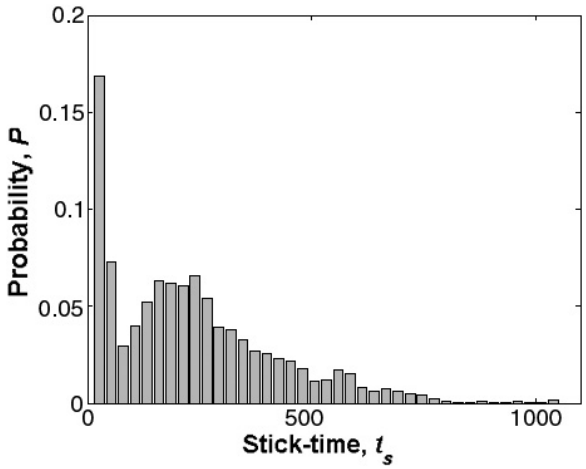

Figure 6. Probability distribution of the sticking times in the hopping regime. Parameter values as in figure 2(b).

in the cloud, and that this asymmetry grows with an increase of the velocity. Our simulations demonstrate that the escape of the bead from a symmetric cloud occurs due to stochastic fluctuations in the local density of filaments around the bead. Figure 1(a) shows a filament distribution at the moment of a spontaneous symmetry-breaking. A strong asymmetry builds up only later as a result of directional motion (figure 1(b)). All of the velocity spikes in figure 5 correlate with a large asymmetry. After an interval of directed motion with a given velocity, the bead is trapped as a result of a stochastic build-up of an almost symmetric cloud (point D). A probability distribution of sticking times (time intervals of trapping events) in the hopping regime is shown in figure 6. A sticking time is defined as a time interval during which the absolute value of the bead velocity is smaller than $10^{-2} f(R_0)/\gamma$. The latter is smaller than

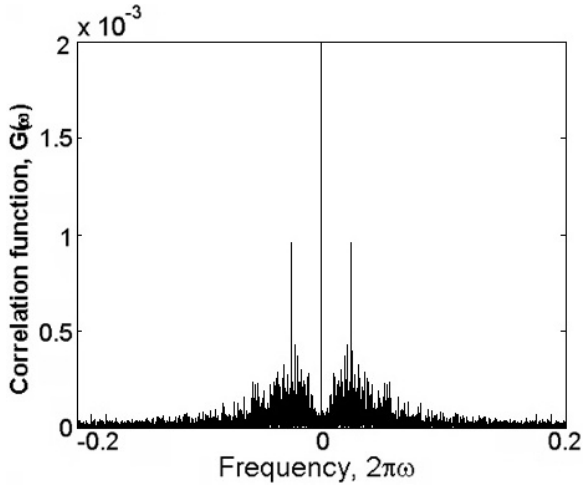

Figure 7. Velocity–velocity correlation function in the hopping regime calculated in the presence of both detached and attached filaments. Parameter values as in figure 2(b).

the maximal velocity in the trapping regime shown in figure 2(c). For small beads which move with higher velocities (see figure 2) a velocity induced asymmetry is strong enough to prevent the formation of symmetric clouds which lead to trapping. It should be noted that the calculated time dependences of the bead velocity, of the cloud asymmetry and of the angular distribution of actin filaments presented in figures 2 and 5 agree qualitatively with the experimental results [2, 4].

Bead dynamics and the nature of filament–bead interactions. The present simulations have been done under the assumption that there are two populations of filaments: attached, which pull the beads, and detached, which push it. Here we assumed that the number of attached filaments is smaller than the number of detached ones. However, it is the presence of the attached filaments which essentially influences the bead motility. We find that the total number of working filaments only slightly changes during the motion of the bead when the bead velocity strongly fluctuates (see figure 5). However, one can see from figure 5 that there is a correlation between the bead velocity and the number of attached filaments; namely, the peaks of the velocity are followed by the minima of the number of attached filaments. The motion of the bead in the hopping regime resembles the stick–slip behaviour observed in friction [18] where adhesive bonds break and reform. In a similar way to stick–slip motion, which originates from a *collective* rupture of the adhesion bonds [19], here hopping motion of the bead is connected to a *collective* rupture of attached filaments.

Analysis of the bead motility in the hopping regime shows that the bead motion in this regime is a stochastic process made of 'free' motions and trapping events. The bead dynamics is characterized by two timescales: a long timescale, t_{l}, corresponding to large jumps (time intervals between maxima of velocity in figure 5), and a shorter timescale, t_{sh}, corresponding to velocity fluctuations (short-range stepping of the bead). In order to isolate the short timescale we have calculated the Fourier transform of the velocity correlation function $G(\omega) = |V(\omega)|^2$, where $V(\omega) = \int_0^\infty \mathrm{d}t\, V(t) \exp(\mathrm{i}\omega t)$; see figure 7. The observed maxima of $G(\omega) = |V(\omega)|^2$ at $\omega = \pm 2 \times 10^{-2}$ correspond to the short-range stepping for which $t_{\mathrm{sh}} = 50$. Using the velocity correlation function for the evaluation of the long timescale requires simulations of very long bead trajectories which are beyond the scope of this work. This timescale is estimated to be

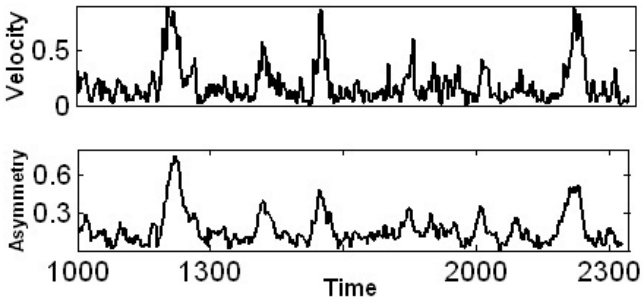

Figure 8. Time dependences of the bead velocity and the cloud asymmetry in the hopping regime calculated in the case when only detached, pushing, filaments exist in the system. Parameter values are as in figure 2(b), except $A_1/A = 0.15$.

$t_l = 1000$ directly from the time series of velocity presented in figure 2. Knowing the values of t_l and t_{sh} we can estimate the length scales of the short-range steps, L_{sh}, and of the large jumps, L_l; namely, $L_{sh} \approx 20\lambda$ and $L_l \approx 400\lambda$. Thus, our simulations suggest a situation of two well separated time and length scales which have been observed in actin-driven systems [4, 20]. It should be noted that in these experiments the ratio of the two length scales was 1000 while in our simulations this ratio equals 20. In order to observe in simulations two length scales which differ by three orders of magnitude one has to perform time-consuming large-scale simulations. This was not the aim of our work. The main idea of this study was to analyse a minimal model that leads to experimentally observed behaviours. Within this model we found two types of length scales which correspond to two different processes: collective detachment–reattachment of filaments, and creation of an almost symmetric actin cloud around the bead (this cloud includes two types of filaments) that leads to trapping of the bead. For the values of the parameters chosen here the ratio of the two lengths is 20; however, for other values of parameters it could be 1000 (which, as mentioned, would require much longer simulations).

In order to clarify the relationships between the observed bead dynamics and the nature of filament–bead interactions, we have performed another set of simulations which is similar to the simulations described above but *does not include attachment* between filaments and the bead surface. Thus, all filaments are assumed to push the bead. Most of the results obtained in this new scenario are qualitatively similar to those discussed above for two types of populations of filaments. Namely, we have also observed here three regimes of bead motion depending on the bead size. Variations of the bead velocity, cloud asymmetry and angular distribution of actin filaments as functions of time look like those presented in figure 2. For instance, figure 8 shows the corresponding results obtained in the hopping regime for the case when only detached, pushing filaments exist in the system. However, calculations of the velocity correlation function as shown in figure 9 demonstrate the absence of the short-timescale behaviour which corresponds to short-range stepping in the case of two populations of filaments (see figure 7). In the presence of the attached filaments these steps were related to unbinding and rebinding between the filaments and bead surface, and this process manifested itself through the characteristic frequency observed in $G(\omega)$.

During the timescale covered by our calculations beads of large radii, $R_0/\lambda > 2.5$, do not escape from the actin cloud and do not produce a 'comet' tail. In this regime the beads perform local random movements characterized by a very small asymmetry of the cloud and an almost uniform angular distribution of filaments (see figure 2(c)). A dependence of time-averaged bead velocity on its radius is shown in figure 10.

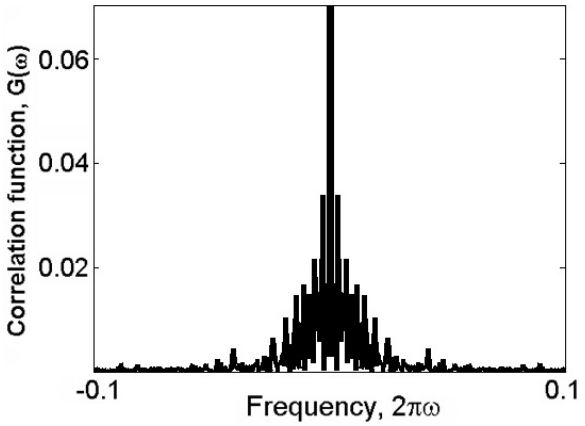

Figure 9. Velocity–velocity correlation function in the hopping regime calculated in the presence of the detached filaments only. Parameter values are as in figure 8.

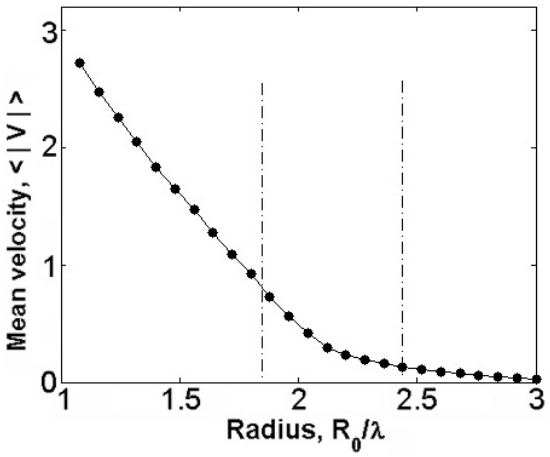

Figure 10. Mean bead velocity as a function of the bead radius. The range of radii for which the hopping motion has been observed is marked by the dash–dot lines. Parameter values as in figure 2.

4. Continuum coarse-grained approach

4.1. Model

The results of the simulations discussed above suggest a coarse-grained description which captures the main features obtained within the microscopic model. We introduce a continuum approach in which the filament subsystem is given in terms of two fields with densities $w_1(\boldsymbol{r})$ and $w_2(\boldsymbol{r})$. These correspond to the barbed ends of the detached and attached filament populations respectively. Namely, the ensemble of discrete points that represented the barbed ends of the filaments within the microscopic model is replaced by smeared density distributions. The dynamics of the fields $w_1(\boldsymbol{r})$ and $w_2(\boldsymbol{r})$ can be described by the kinetic equations in the appendix. Here, in order to illustrate the continuum approach, we consider the case where only one field $w_1(\boldsymbol{r})$, corresponding to the detached filament, is present in the system. The

dynamical equation for $w_1(\boldsymbol{r})$ reads

$$\frac{\mathrm{d}w_1}{\mathrm{d}t} = D_1 \Delta w_1(\mathbf{r}) + Q(\mathbf{R}-\mathbf{r})\,(1+\xi(\mathbf{r},t)) - \mu w_1(\mathbf{r}). \tag{6}$$

Here the function Q presents a nucleation of the detached filaments around the bead (below we assume that Q is a constant, Q_0, in the ring of width ΔR_0), the random function ξ is δ correlated and represents the effect of noise on the nucleation; the coefficient μ accounts for a degradation of the filament population, and the coefficient D_1 defines the diffusion rate due to the Brownian motion of the filaments. Including the noise contribution in the nucleation term is essential for the observation of the spontaneous symmetry-breaking phenomenon and of the nonstationary regimes of bead motion.

The motion of the bead is described by the macroscopic equation, equation (4), where the effect of the filaments on the bead is given by the integral force

$$F = \int \mathrm{d}\mathbf{r}'\, F_1\left(\mathbf{R}-\mathbf{r}'\right) w_1\left(\mathbf{r}'\right), \tag{7}$$

and the force kernel F_1 has the same form as in equation (5).

The analysis of equations (6) and (7) shows that there is a direct relationship between the bead velocity and the spatial asymmetry of the density w_1. For a bead moving with constant velocity V the macroscopic equation (4) reduces to a relation between the velocity and the density w_1

$$V = \frac{1}{\eta}\int \mathrm{d}\mathbf{r}'\, F_1\left(\mathbf{R}-\mathbf{r}'\right) w_1\left(\mathbf{r}'\right). \tag{8}$$

It should be noted that the kernel F_1, which is the gradient of the potential, is an asymmetric function along every line passing through the centre of the bead. As a result, the isotropic part of the filament density w_1 does not influence the bead velocity. In turn, for a given constant velocity the density w_1 can be found from equation (6), which after the substitutions

$$\tilde{\mathbf{r}} = \mathbf{r}-\mathbf{R}, \qquad \tilde{w}_1\left(\tilde{\mathbf{r}},\mathbf{V}\right) = w_1 \exp\left(\mathbf{V}\tilde{\mathbf{r}}/D_1\right), \qquad \tilde{\mu} = \mu + V^2/4D_1,$$
$$\tilde{Q}\left(\tilde{\mathbf{r}},\mathbf{V}\right) = Q\exp\left(\mathbf{V}\tilde{\mathbf{r}}/D_1\right),$$

transforms into the equation for a steady distribution $\tilde{w}_1$

$$D_1 \Delta \tilde{w}_1(\tilde{\mathbf{r}}) + \tilde{Q}(\tilde{\mathbf{r}}) - \tilde{\mu}\tilde{w}_1(\tilde{\mathbf{r}}) = 0. \tag{9}$$

Here, for a bead moving with a constant velocity, we neglect the randomness of the nucleation process. The validity of this assumption is supported by numerical results presented in appendix. The formal solution of the above equation can be written in the form

$$\tilde{w}_1(\tilde{\mathbf{r}}) = \int \mathrm{d}\mathbf{q}\, \frac{\exp\left(-\mathrm{i}\mathbf{q}\tilde{\mathbf{r}}\right)\tilde{Q}(\mathbf{q},\mathbf{V})}{D_1 q^2 + \tilde{\mu}}. \tag{10}$$

For a given set of parameters the coupled equations (8) and (10) define self-consistently the unique bead velocity and the structure of the filament cloud. Figure 11 shows an example for a density profile w_1 in the case of a nonzero bead velocity which has been numerically calculated using equation (10) for a one-dimensional model. The asymmetry of the profile grows self-consistently with the increase of velocity. A grey-scale map of a 2D filament density distribution around the moving bead is shown in figure 12. This figure clearly shows a propulsive structure of the actin tail, which has been observed in biomimetic measurements [4].

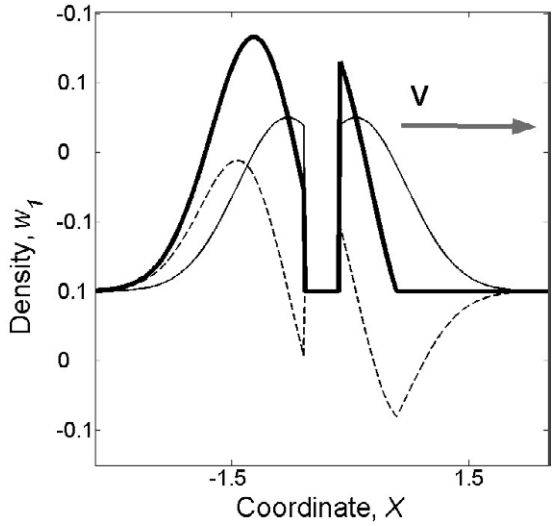

Figure 11. An example of a density profile w_1 for a nonzero bead velocity (bold line) which has been numerically calculated within a one-dimensional continuum model using equation (9). The thin line shows the density profile corresponding to zero bead velocity, and the dashed line represents a velocity induced contribution, $(V/\mu)\,\mathrm{d}Q/\mathrm{d}r$, to w_1 for a nonzero velocity. Coordinates and density are presented in units of λ and Q_0/μ, respectively. Parameter values: the amplitude of the noise in the nucleation channel, $\sigma = 1.25$, $D_1/(U_0\lambda^2) = 0.1$, $R_0/\lambda = 0.43$, $\Delta R_0 = 0.5\lambda$.

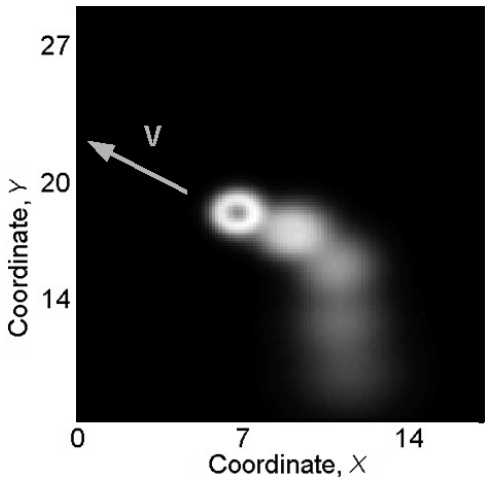

Figure 12. A grey-scale map of a 2D filament density distribution around the moving bead calculated within the continuum approach. Parameter values: $\sigma = 1.25$, $D_1/(U_0\lambda^2) = 0.1$, $R_0/\lambda = 0.43$, $\Delta R_0 = 0.5\lambda$, $6\pi\eta\lambda\mu/A_1 = 7$, $k_\mathrm{B}T/(A_1R_0^3) = 10^{-2}$.

4.2. Results of calculations

The qualitative conclusions of the coarse-grained model are similar to that obtained within the microscopic approach discussed above. The continuum model also exhibits the phenomenon of spontaneous symmetry-breaking and three different regimes of motion depending on the size of the bead, as in the case of the microscopic description. We will not repeat here a

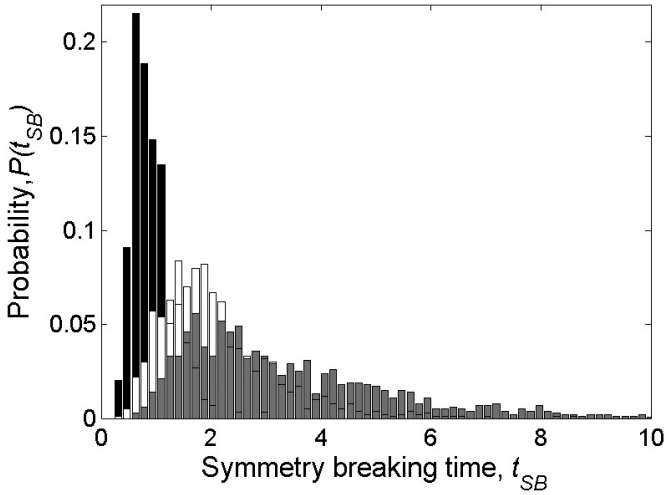

Figure 13. Probability distribution function histograms of symmetry-breaking times calculated for three bead radii, R_0/λ: 0.35—black, 0.60—white, and 0.70—grey. Calculations have been performed according to equations (A.1)–(A.3). Time is presented in units of $1/\mu$. Parameter values are as in figure 12, except $D_2 = D_1$, $\beta = 0.5$, $\mu_{21} = \mu$, $K = A_1$, and $\mu_{12}(\mathbf{R} - \mathbf{r}) = 2\mu \exp(7|\mathbf{R} - \mathbf{r}|/\lambda)$.

detailed discussion of these behaviours, which have already been presented in the previous section, and will focus on two phenomena that have not been discussed within the microscopic model: symmetry-breaking, and how it varies with the radius of the bead, and the viscosity dependence of the bead velocity. Both problems have been investigated experimentally, but the data and their theoretical interpretations are still controversial [3–6, 21].

4.2.1. Spontaneous symmetry-breaking. Both the microscopic and continuum models show that no intrinsic asymmetry is required for directed motion. In our model spontaneous symmetry-breaking is caused mainly by the stochastic nature of the nucleation and polymerization that lead to a favourable (spontaneous) asymmetric fluctuation in the spatial distribution of filament density. The effect of the bead Brownian motion on the symmetry-breaking is less important. This instantaneous asymmetry of the density distribution results in a net force that pushes the bead out of the actin cloud. This is followed by a stabilization of the asymmetry by *the* directed velocity (see equation (10)). Thus, in spite of spherical symmetry of the system, the model exhibits a spontaneous symmetry-breaking followed by a stable directed motion with an almost constant velocity for a broad range of parameters. For small bead radii and low viscosities the time intervals of the directed motion can be very long. Figure 13 shows the probability distribution functions (pdfs) for symmetry-breaking times, T_{sb}, calculated for three bead radii. With an increase in the bead radius not only does the mean value of T_{sb} increase but also the width of the time distribution. Therefore, measuring only the mean value, T_{sb}, can be misleading. It is the whole pdf of T_{sb} that contributes to the understanding the mechanism of motility.

4.2.2. Velocity–viscosity relations. Figure 14 shows a time averaged bead velocity, $\langle |V| \rangle$, and the fraction of time that the bead spends in a slippage state as a function of the viscosity. The term 'slippage' we borrow from the stick–slip phenomenon, which resembles the bead's

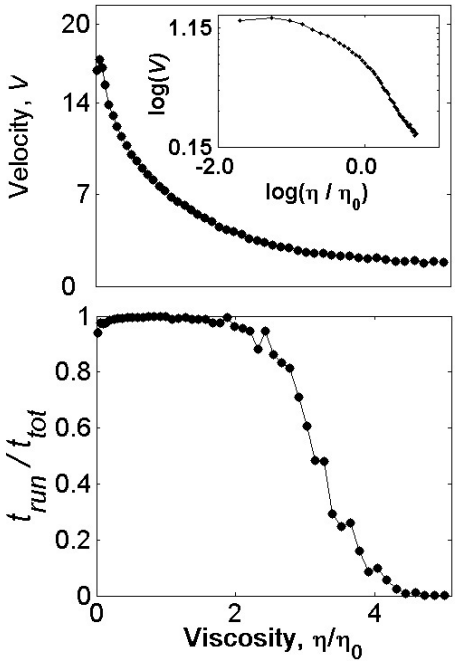

Figure 14. Time averaged bead velocity, and fraction of time that the bead spends in a slippage state as a function of viscosity of the surrounding medium. The velocity is presented in units of $\lambda\mu$. Parameters are as in figure 13, except $R_0/\lambda = 0.43$ and $\eta_0 = A_1/(\pi\lambda\mu)$.

motion. We note that the mean velocity in the hopping regime, $2\eta/\eta_0 < 4$, has been calculated considering only time intervals during which the bead moves, ignoring the local sticking times. The inset to figure 14 presents the viscosity dependence of $\langle|V|\rangle$ plotted on a log–log scale.

In the regime of steady motion, $\eta/\eta_0 < 2$, the curve $\langle|V|\rangle$ versus η/η_0 displays two distinct behaviours at small and large viscosities correspondingly. At small viscosities the mean velocity is almost independent of η/η_0, while for larger η/η_0 there is a significant decrease in $\langle|V|\rangle$. This behaviour can be explained taking into account that for small η/η_0 the external resistive force due to a viscous friction is smaller than the internal resistive force due to pulling attached filaments [5]. In this interval of η/η_0, we obtain that $\langle|V|\rangle$ only slightly decreases with η/η_0. This behaviour is in agreement with observations [5] that find almost no slowing down of beads when the viscosity is increased 4000-fold. For higher values of η/η_0, when the resistance is dominated by viscous force, the mean velocity decreases essentially with η.

In the hopping regime $\langle|V|\rangle$ again decreases slowly with the viscosity. The latter can be explained by the fact the velocity with which a bead leaves a trapped state is determined by the height of the barrier created by the symmetric actin cloud and does not depend on viscosity. As a result the mean bead velocity during slippage intervals only slightly depends on η/η_0, but the time fraction of the slippage intervals decreases sharply with η/η_0 (see figure 14(b)).

A biphasic behaviour of $\langle|V|\rangle$ versus η/η_0 with a significant reduction of $\langle|V|\rangle$ for small values of η/η_0, and a slower decrease of $\langle|V|\rangle$ for higher values of η/η_0, has been observed in [21], which seems to contradict the very weak dependence of $\langle|V|\rangle$ on η/η_0 found in [5]. Within our approach this marked difference might correspond to different regimes of motion. In order to understand the nature of the observed phenomena one has to analyse the time series of the velocity, since the behaviour of the mean value of velocity does not always provide meaningful information on the mechanisms of force generation and motility.

5. Conclusions

We have proposed a microscopic model for the bead motility driven by the polymerization of actin filaments. The model includes two types of filaments (detached and attached) that grow in the vicinity of a spherical bead which is propelled by the formation of a filament tail. Our findings suggest a simple coarse-grained description which captures the main features obtained for the microscopic model. Both the microscopic and continuum models show that intrinsic asymmetry is not required for a directional motion defined between switching events. In spite of the spherical symmetry of the system the model exhibits a spontaneous symmetry-breaking followed by a stable directed motion for a broad rage of parameters. In our models a spontaneous symmetry breaking is caused mainly by the stochastic nature of the nucleation and polymerization that lead to a favourable asymmetric fluctuation in the spatial distribution of the filament density. The effect of the bead Brownian motion on a symmetry-breaking is negligible here.

The models exhibit a rich spectrum of behaviours which have been observed in biomimetic experiments [2–6, 21], such as spontaneous symmetry-breaking, various regimes of the bead motion and correlations between the structure of the actin tail and the bead dynamics. The obtained dependences of the system dynamical properties (the symmetry-breaking time, regimes of motion, mean velocity, tail asymmetry, and others) on the physical parameters (the bead radius and viscosity) agree well with the experimental observations.

We found that most experimental observations can be reproduced taking into account only one type of filaments interacting with the bead—the detached filaments that push the bead. However, in the absence of attached filaments the system does not exhibit fine structure in the fluctuations of the velocity, which correspond to short steps. Our calculations suggest that measurements of the velocity correlation function could provide important information on the mechanism of motility. In particular, the presence of high-frequency peaks in $G(\omega)$ indicates the role of the attached filament in bead dynamics. Unfortunately, an absence of the high-frequency peaks in $G(\omega)$ cannot serve as an unambiguous proof for the absence of attached filaments.

In addition, the analysis of mean characteristics only (velocities, symmetry breaking times etc) does not always provide meaningful information about the mechanism of motility. The aim should be obtaining the whole distributions, which might be extremely broad.

In general, the observed motion of the bead can be described and analysed in the framework of a random walk process whose details are related to the distributions obtained in the microscopic model. Namely, viewing the motion of the bead as a random walk, one can obtain these distributions from analysing the trajectory, provided it is long enough. From the trajectory the distribution of persistent lengths (which give some idea of directionality) can be obtained, as well as the distribution of sticking times (local fluctuations). More complicated is the angular aspect, where angular correlations can be defined that provide information on directional changes. This random walk approach we believe can correlate the observed motion and the underlying microscopic quantities [22].

Appendix

Within a continuum approach the dynamics of the field densities $w_1(\boldsymbol{r})$ and $w_2(\boldsymbol{r})$, which correspond to the detached and attached filament populations respectively, can be described by the following kinetic equations:

$$\frac{\mathrm{d}w_1}{\mathrm{d}t} = D_1 \Delta w_1(\mathbf{r}) + [(1-\beta) Q(\mathbf{R}-\mathbf{r})(1+\xi(\mathbf{r},t)) - \mu w_1(\mathbf{r}) - \mu_{12}(\mathbf{R}-\mathbf{r}) w_1(\mathbf{r}) + \mu_{21} w_2(\mathbf{r})] \tag{A.1}$$

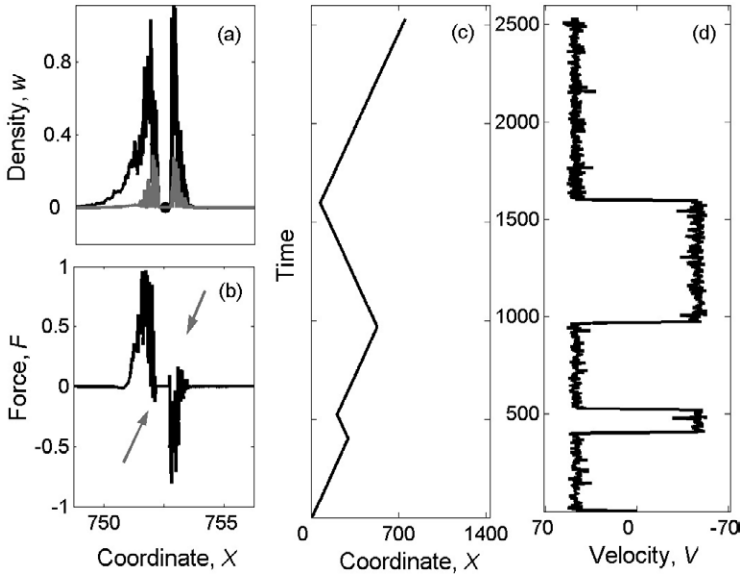

Figure A.1. (a) Instantaneous density profiles for detached (black) and attached (grey) filaments, (b) the corresponding spatial distributions of the force density acting on the bead, (c) typical bead trajectory, and (d) time series of the bead velocity for a regime of steady motion (with a few turning points) calculated for a one-dimensional continuum system. Parameters are as in figure 13, except $R_0/\lambda = 0.43$.

$$\frac{\mathrm{d}w_2}{\mathrm{d}t} = D_2 \Delta w_2(\mathbf{r}) + [\beta Q(\mathbf{R}-\mathbf{r})(1+\xi(\mathbf{r},t)) - \mu w_2(\mathbf{r}) - \mu_{21} w_2(\mathbf{r}) + \mu_{12}(\mathbf{R}-\mathbf{r}) w_1(\mathbf{r})]. \tag{A.2}$$

Here the functions $(1-\beta)Q$ and βQ present a nucleation of detached and attached filaments in a ring around the bead, respectively; the δ-correlated random function $\xi(\boldsymbol{r}, t)$ simulates the role of noise in the nucleation process; the coefficients μ, μ_{12} and μ_{21} account for a degradation of the filament populations (relaxation) and for the mutual transitions between the two populations. As in the microscopic model, we assume an exponential increase of the detachment rate μ_{12} with a distance from the bead. The coefficients D_1 and D_2 define the diffusion rates for two types of filaments. Including the noise contribution to the nucleation term is essential for the observation of the spontaneous symmetry-breaking phenomena and nonstationary regimes of bead motion.

$$F = \int \mathrm{d}\mathbf{r}' \left(F_1\left(\mathbf{R}-\mathbf{r}'\right) w_1\left(\mathbf{r}'\right) + F_2\left(\mathbf{R}-\mathbf{r}'\right) w_2\left(\mathbf{r}'\right)\right), \tag{A.3}$$

and the force kernels F_1 and F_2 have the same form as in equation (5). In the case when only one field w_1 which corresponds to the detached filaments exists in the system, equations (A.1)–(A.3) reduce to equations (6), (7) in the text.

In figure A.1 we show only a typical bead trajectory, $X(t)$, and a time series of the bead velocity for the regime of steady motion (with a few turning points) calculated using equations (4) and (A.1)–(A.3) for a one-dimensional system. Figure A.1(a) also presents instantaneous density profiles for detached and attached filaments, w_1 and w_2, and the corresponding spatial distribution of the force density acting on the bead. The net force experienced by the bead is an integral of the force density in figure A.1(a). An asymmetry in the densities w_1 and w_2 leads to a nonzero net force for the moving bead. The effect of

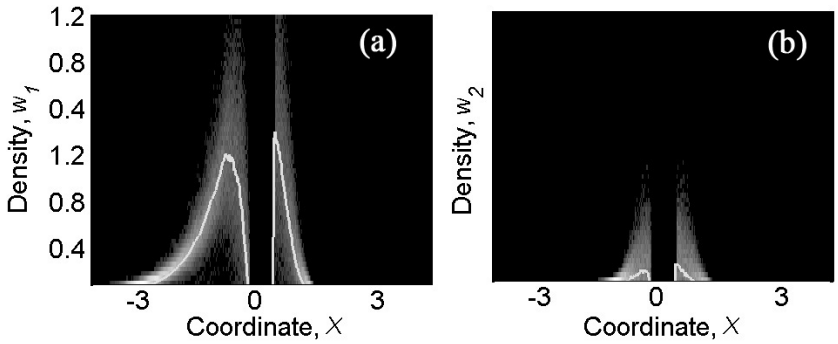

Figure A.2. The grey-scale maps show pdfs for the time averaged densities of (a) detached and (b) attached filaments for a bead moving in the positive direction. The white lines present the corresponding mean values at each coordinate. Parameters are as in figure A.1.

attached filaments producing a resistive force is reflected by minima in the force density (with a sign opposite to the contribution of the detached filaments) which is marked by an arrow in figure A.1(a). The grey-scale maps in figure A.2 show the pdfs for the time averaged densities of the attached and detached filaments for a bead moving in the positive direction, and the white lines present the corresponding mean vaues. The calculated mean density w_1 is well described by the approximate solution, equation (10), displayed in figure 11, which has been derived ignoring the noise contribution to the nucleation process.

References

[1] Bray D 2001 *Cell Movements* 2nd edn (New York: Garland)
[2] Cameron L A, Footer M J, van Oudenaarden A and Theriot J A 1999 *Proc. Natl Acad. Sci. USA* **96** 4908
[3] van Oudenaarden A and Theriot J A 1999 *Nat. Cell Biol.* **1** 493
[4] Bernheim-Groswasser A, Wiesner S, Golsteyn R M, Carlier M F and Sykes C 2002 *Nature* **417** 308
[5] Wiesner S, Helfer E, Didry D, Ducouret G, Lafuma F, Carlier M F and Pantaloni D 2004 *J. Cell Biol.* **160** 387
[6] Upadhyaya A and van Oudenaarden A 2003 *Curr. Biol.* **13** R734
[7] Tilney L G and Portnoy D A 1989 *J. Cell Biol.* **109** 1597
[8] Cameron L A, Giardini P A, Soo F S and Theriot J 2000 *Nat. Rev. Mol. Cell Biol.* **1** 110
[9] Mogilner A and Oster G 1996 *Biophys. J.* **71** 3030
[10] Mogilner A and Oster G 2003 *Biophys. J.* **84** 1591
[11] Mogilner A and Oster G 2003 *Cur. Biol.* **13** R721
[12] Carlsson A E 2001 *Biophys. J.* **81** 1907
Carlsson A E 2003 *Biophys. J.* **84** 2907
[13] Gerbal F, Chaikin P, Rabin Y and Prost J 2000 *Biophys. J.* **79** 2259
[14] Bottino D, Mogilner A, Roberts T, Stewart M and Oster G 2002 *J. Cell. Sci.* **115** 367
[15] Joanny J-F, Julicher F and Prost J 2003 *Phys. Rev. Lett.* **90** 168102
[16] Sekimoto K, Prost J, Julicher F, Boukellal H and Bernheim-Grosswasser A 2004 *Eur. Phys. J.* E **13** 247
[17] Evans E 2001 *Annu. Rev. Biophys. Biomol. Struct.* **30** 105
[18] Urbakh M, Klafter J, Gourdon D and Israelachvili J 2004 *Nature* **430** 525
[19] Filippov A E, Klafter J and Urbakh M 2004 *Phys. Rev. Lett.* **9** 135503
[20] Kuo S C and McGrath J L 2000 *Nature* **407** 1026
[21] McGrath J L, Eungdamrong N J, Fisher C I, Peng F, Mahadevan L, Mitchison T J and Kuo S C 2003 *Curr. Biol.* **13** 329
[22] Weiss G H 1994 *Aspects and Applications of the Random Walk* (Amsterdam: North-Holland)